
**Liquid Crystals**
Publication details, including instructions for authors and subscription information:
http://www.informaworld.com/smpp/title~content=t713926090

# Characterization, optical and thermal properties of new azomethines based on heptadecafluoroundecyloxy benzaldehyde

Agnieszka Iwan[a]; Henryk Janeczek[b]; Bozena Jarzabek[b]; Marian Domanski[b]; Patrice Rannou[c]
[a] Division of Electrotechnology and Materials Science, Electrotechnical Institute, Wroclaw, Poland [b] Centre of Polymer and Carbon Materials, Polish Academy of Sciences, Zabrze, Poland [c] Laboratoire d'Electronique Moléculaire, Organique et Hybride, UMR5819-SPrAM (CEA-CNRS-Univ. J. FOURIER-Grenoble I), INAC Institut Nanosciences and Cryogénie, CEA-Grenoble, Grenoble Cedex 9, France

**To cite this Article** Iwan, Agnieszka , Janeczek, Henryk , Jarzabek, Bozena , Domanski, Marian and Rannou, Patrice(2009) 'Characterization, optical and thermal properties of new azomethines based on heptadecafluoroundecyloxy benzaldehyde', Liquid Crystals, 36: 8, 873 — 883
**To link to this Article: DOI:** 10.1080/02678290903100539
**URL:** http://dx.doi.org/10.1080/02678290903100539

*Liquid Crystals,*
Vol. 36, No. 8, August 2009, 873–883

Taylor & Francis
Taylor & Francis Group

# Characterization, optical and thermal properties of new azomethines based on heptadecafluoroundecyloxy benzaldehyde

Agnieszka Iwan[a]*, Henryk Janeczek[b], Bozena Jarzabek[b], Marian Domanski[b] and Patrice Rannou[c]

[a]*Electrotechnical Institute, Division of Electrotechnology and Materials Science, M. Sklodowskiej-Curie 55/61 Street, 50-369 Wroclaw, Poland;* [b]*Centre of Polymer and Carbon Materials, Polish Academy of Sciences, 34 M. Curie-Sklodowska Street, 41-819 Zabrze, Poland;* [c]*Laboratoire d'Electronique Moléculaire, Organique et Hybride, UMR5819-SPrAM (CEA-CNRS-Univ. J. FOURIER-Grenoble I), INAC Institut Nanosciences and Cryogénie, CEA-Grenoble, 17 Rue des Martyrs, 38054 Grenoble Cedex 9, France*

*(Received 16 March 2009; final form 8 June 2009)*

New thermotropic liquid crystals containing a long alkoxysemiperfluorinated chain (-O-$(CH_2)_3$-$(CF_2)_7$-$CF_3$), one linking unit in mesogenic cores (HC=N-) and different functional end-groups such as 4-hexadecyl-, 4-n-hexadecyloxy- chain, or biphenyl-4-carbonitrile, 4-diazenyl-N,N-dimethylbenzene or pyren were synthesized via a one-step route. The methods of nuclear magnetic resonance (NMR), Fourier transform infrared (FTIR), ultraviolet–visual (UV-vis) and photoluminescence (PL) spectroscopy as well as differential scanning calorimetry (DSC) and polarizing optical microscopy (POM) were used. The absorption (UV-vis) and PL features of all compounds are documented. The amine had an effect on the mesomorphic properties of the azomethines. An enantiotropic smectic phase was observed for all of the systems studied. As a result of DSC and POM investigations, it is shown that liquid crystalline properties of the azomethines exhibit a strong dependence of the end-groups. The mesomorphic behaviour of the compounds was investigated also by FTIR(T) and UV-vis(T) spectroscopy. Current–voltage measurements were performed on an ITO/compound/$Alq_3$/Al device.

**Keywords:** azomethines; liquid crystals; heptadeca fluoroundecyloxy benzaldehyde; photoluminescence; current-voltage measurements



## 1. Introduction

The subject of liquid crystals (LCs) and their applications in electronic displays and in non-linear optical systems has become of huge importance during the last two decades. LCs have wide application in devices such as computer displays, wherein thin films of liquid crystals are sandwiched between two glass surfaces that have electrodes printed on their surfaces (*1, 2*). The LCs display industry has a yearly turnover of more than US$10 billion (*1*). The liquid crystalline materials are dividing according to Samulski terminology for monomer liquid crystals (MLCs) and polymer liquid crystals (PLCs) (*2*). It was also specified that a MLCs compounds can or cannot polymerize.

The fluoro substituent in organic compounds such as oligomers and polymers is very interesting because of the combination of polar and steric effects and the great strength of the C–F bond which confers stability on fluoro-substituted compounds. Fluorine has the highest electronegativity (3.98) of all of the elements such as H, Cl, Br, I, C, N, O and, hence, as a substituent confers a high dipole moment on the C–F bond (*3*). Moreover, the fluoro substituent has a low polarizability ($5.57/10^{25}$ $cm^{-1}$) which confers low intermolecular dispersion interactions. The fluoro substituent is the smallest, after hydrogen, of all possible substituents and is monoatomic. The size influence is not too large, which enables it to be usefully incorporated into parent molecules for beneficial modification of properties. The bulky nature of the neighbouring fluoro substituents causes steric interactions which tend to limit conformational flexibility and, hence, perfluoro chains are often described as stiff (*3*). The low polarizability of fluorine confers weak intermolecular forces of perfluoro systems which results in very low surface tension of liquids and very low surface energy on perfluorinated solids (*3*). There have been relatively few studies dedicated to enhancing the polarizability and dipole moments of LCs using the hypervalent $SF_5$ group (*4*). To reduce the rotational viscosities of the $SF_5$-based azomethines, Smith *et al.* (*5*) selected a fluorocarbon spacer to separate the $SF_5$ group from the aromatic ring structure ($SF_5$-$CF_2$-$CF_2$). Two alkoxyaldehydes (OHC-$C_6H_4$-O-$C_7H_{15}$ and OHC-$C_6H_4$-O-$C_{10}H_{21}$) were condensation with meta- and para-amine ($SF_5$-$CF_2$-$CF_2$-$C_6H_4$-$NH_2$). Attachment of an $SF_5$ group separated from a benzylidine group by a fluorinated spacer leads to monotropic nematic and smectic phases, while an enantiotropic nematic phase was observed in mixtures (*5*). In addition, the azomethine dimers with lateral fluorine substituents on the core and/or on the outer

*Corresponding author. Email: a.iwan@iel.wroc.pl

ISSN 0267-8292 print/ISSN 1366-5855 online

DOI: 10.1080/02678290903100539
http://www.informaworld.com

rings were investigated (*6–9*). Moreover, LCs based on semiperfluorinated imines and salicylaldimato metal complexes were investigated by Bilgin-Eran *et al.* (*10*). They found that the thermal behaviour of the semiperfluorinated imines depends on the number of chain, the substitution pattern and the number of fluorine atoms in the fluoroalkyl chains. Along with increasing the number of F atoms in the fluoroalkyl chains stabilization of smectic and columnar mesophases was observed (*10*).

In addition, many scientists have investigated the influence of the fluoro substituents or chain fluorination on the LC properties of different classes of mesogens (*3, 11–42*). Mainly, fluoro substituents were investigated in the terminal chains of oligomers (*3, 11–23*), discotic LCs (*3, 24–29*), supramolecular LCs (*3, 30, 31*) and in lyotropic LCs and biological significance (*3, 32–37*). As an example, we name a few: semifluorinated Janus-dendritic benzamides (*28*), hexabenzocoronenes bearing perfluorinated chains (*26*) or perfluorinated supramolecular dendrimers containing an ester (-$COOCH_3$) head group, a rigid biphenylene group and three perfluorinated (-$CF_3$) tails (*29*).

Here, we report the investigation of five azomethines with a long alkoxysemiperfluorinated chain (-O-$(CH_2)_3$-$(CF_2)_7$-$CF_3$) and different functional end-groups. The structure–property relations were studied by changing the functional end-groups. In accordance with the best of our knowledge the absorption properties of the azomethines with semiperfluorinated chains in the function of temperature have not been investigated so far.



## 2. Experimental details

### 2.1 Materials

Acetone, ethanol, N,N-dimethylacetamide (DMA) (Aldrich) and 4-(4,4,5,5,6,6,7,7,8,8,9,9,10,10,11,11,11-heptadecafluoroundecyloxy)benzaldehyde (Fluka), 4-hexadecylaniline (Aldrich), 4-n-hexadecyloxyaniline (Aldrich), 4'-aminobiphenyl-4-carbonitrile (Aldrich), 4-((4-aminophenyl)diazenyl)-N,N-dimethylbenzenamine (Aldrich), pyren-1-amine (Aldrich) were used without any purification.

### 2.2 Characterization techniques

All synthesized compounds were characterized by $^1H$ and $^{13}C$ nuclear magnetic resonance (NMR) and elemental analysis. Compounds were also characterized by Fourier transform infrared attenuated total reflection (FTIR-ATR) and ultraviolet–visible (UV-vis) absorption spectroscopy. Compounds were subjected to fluorescence spectroscopy. NMR was recorded on a Bruker AC 200 MHz. Chloroform-*d* ($CDCl_3$) containing tetramethylsilane (TMS) as an internal standard were used as solvent. Elemental analyses (C, H and N) were recorded on a 240C Perkin-Elmer analyser. FTIR spectra of the compounds were recorded on a Perkin-Elmer paragon 500 spectrometer (wavenumber range: 400–4000 $cm^{-1}$; resolution: 2 $cm^{-1}$). Solution (tetrahydrofuran (THF)) UV-vis absorption spectra were recorded *in situ* during the size exclusion chromatography (SEC) analyses using the diode array UV-vis spectrometer of the 1100HP Chemstation and on a Perkin-Elmer Lambda 2 spectrometer, respectively. Two runs of 20 μl injection of around 0.5 mg $ml^{-1}$ Compounds in high-performance liquid chromatography (HPLC) grade THF solutions were typically analysed for each sample with a UV-vis detection located at 325 nm.

PL THF solution spectra were carried out on a Jobin-Yvon HR 550 monochromator equipped with a CCD silicon detector cooled to 140 K (325 nm excitation line).

Current–voltage measurements were performed on an ITO/compound/$Alq_3$/Al device. The azomethine solution (1 w/v% in dichloroethane) was spin-cast onto ITO-covered glass substrate at room temperature. Residual solvent was removed by heating the film in a vacuum. An $Alq_3$ layer was prepared on the polymer film surface by vacuum deposition at a pressure of $2 \times 10^{-4}$ Pa and then the Al electrode was vacuum deposited at the same pressure. The area of the diodes was 9 $mm^2$. Current–voltage characteristics were detected using an electromether Keithey 6715.

The phase transitions and mesogenicity were studied by differential scanning calorimetry (DSC) and polarizing optical microscopy (POM) observations. DSC were measured on a TA-DSC 2010 apparatus using sealed aluminium pans under nitrogen atmosphere at a heating/cooling rate of 0.5°C $min^{-1}$ in a temperature range from –20°C to over the clearing point.

The textures of the liquid-crystalline phase were observed with a POM set-up composed of: (i) a LEICA DMLM Microscope (magnification 2.5×, 5×, 10×, 20× and 50×) working in both transmission and reflexion modes; (ii) LINKAM LTS350 (–196°C to +350°C) hot plate and LINKAM CI94 temperature controller; (iii) JVC Numeric 3-CCD KYF75 camera (resolution: 1360 × 1024). The temperature dependence of the FTIR spectra was measured for powders using a Perkin-Elmer paragon 500 spectrometer using a temperature-controlled optical cell in the temperature range from the clearing point to room temperature in the cooling process. The temperature dependence of the UV-vis spectra was measured for thin films on the glass (film cast from dichloroethane) using JASCO V-570 UV-Vis-NIR (near infrared)

spectrometer using a temperature-controlled optical cell in the temperature range from room temperature to the clearing point in the heating process.

### *2.3 General synthetic procedure of compounds 1–5*

A mixture of aldehyde (1.0 mmol) and amine (1.0 mmol) in DMA solution in the presence of *p*-toluenesulfonic acid (PTS) (0.06 g) was refluxed with stirring for 10 hours. The reaction was conducted in an argon atmosphere and the condenser was fitted with a Dean–Stark trap. After cooling, the mixture was precipitated with 100 ml of ethanol. The crude product was washed three times with methanol (3 × 500 ml) and then twice with acetone (2 × 350 ml) to remove unreacted monomers. Then the compound was dried at 60°C under vacuum for 12 hours.

#### *2.3.1 N-(4-(4,4,5,5,6,6,7,7,8,8,8,9,9,10,10,11,11,11 heptadecafluoroundecyloxy)benzylidene)-4-hexadecylbenzenamine* (**1**)

Yield: 87%. Melting point (heating rate 10°C $min^{-1}$): 110°C. FTIR-ATR: $\nu_{max}$ in $cm^{-1}$ 2918, 2850, 2354, 2333, 1624 (HC=N), 1596, 1561, 1508, 1463, 1372, 1245, 1196, 1140, 1063, 1021, 832, 712, 649. $^1$H NMR (200 MHz, $CDCl_3$, TMS) [ppm]: $\delta$ 8.45 (s, 1H, C**H**=N-); 7.89 (s, 2H, $\mathbf{H_{Ar}}$-CH=N); 7.15-7.26 (m, 4H, $\mathbf{H_{Ar}}$); 7.02 (s, 2H, $\mathbf{H_{Ar}}$-O); 4.13-4.18 (m, 2H, C$\mathbf{H_2}$–O); 2.62-2.69 (m, 2H, C$\mathbf{H_2}$–Ar); 2.26-2.36 (m, 2H, $CH_2$-C$\mathbf{H_2}$– $CH_2$-$CF_2$); 2.15-2.25 (m, 2H, C$\mathbf{H_2}$–$CF_2$); 1.62-1.66 (m, 2H, C$\mathbf{H_2}$-$CH_2$-Ar); 1.30-1.33 (m, 26H, -(C$\mathbf{H_2}$)$_{13}$-$CH_3$); 0.89-0.95 (m, 3H, C$\mathbf{H_3}$). $^{13}$C NMR (50 MHz, $CDCl_3$, TMS) [ppm]: $\delta$ 161.12 (-**C**H=N-), 158.79 ($\mathbf{C_{Ar}}$-O-), 149.51 ($\mathbf{C_{Ar}}$-N=CH-), 140.72 ($\mathbf{C_{Ar}}$-$(CH_2)_{15}$-$CH_3$), 132.02 ($\mathbf{C_{Ar}}$, orto position to HC=N-), 130.57 ($\mathbf{C_{Ar}}$, orto position to -$(CH_2)_{15}$-$CH_3$), 129.58 ($\mathbf{C_{Ar}}$, orto position to N=CH-), 129.09 ($CH_2$-$CF_2$-**C**$F_2$-$CF_2$), 128.58 ($\mathbf{C_{Ar}}$-CH=N-), 120.76 (**C**$F_2$-$CH_2$), 119.52 (**C**$F_3$), 115.19 ($\mathbf{C_{Ar}}$, orto position to -O-), 114.60 -(**C**$F_2$)$_3$-$CF_2$-$CF_2$-$CF_3$), 109.28 ((**C**$F_2$)$_2$-$CF_3$), 66.40 (**C**$H_2$-O-), 35.51 (**C**$H_2$-Ar), 31.93 (**C**$H_2$-$CH_2$-Ar), 29.70 ((**C**$H_2$)$_{11}$-$(CH_2)_2$-Ar), 27.91 ($CH_2$-**C**$H_2$-$CF_2$), 22.70 (**C**$H_2$-$CH_3$), 20.53 (-O-$CH_2$-**C**$H_2$-$CH_2$-$CF_2$), 14.11 **C**$H_3$). Analysis calculated for $C_{40}H_{48}F_{17}NO$: C, 54.48%; H, 5.49%; N, 1.59%. Found: C, 54.64%; H, 5.46%; N, 1.60%.

#### *2.3.2 N-(4-(4,4,5,5,6,6,7,7,8,8,8,9,9,10,10,11,11,11 heptadecafluoroundecyloxy)benzylidene)-4-(hexadecyloxy)benzenamine* (**2**)

Yield: 89%. Melting point (heating rate 10°C $min^{-1}$): 115°C. FTIR-ATR: $\nu_{max}$ in $cm^{-1}$ 2918, 2850, 2347, 2319, 1619 (HC=N), 1602, 1577, 1510, 1471, 1291, 1243, 1195, 1140, 1114, 1017, 973, 841, 709, 643. $^1$H NMR (200 MHz, $CDCl_3$, TMS) [ppm]: $\delta$ 8.44 (s, 1H, C**H**=N-); 7.87 (s, 2H, $\mathbf{H_{Ar}}$-CH=N); 6.93-7.30 (m, $\mathbf{H_{Ar}}$); 4.12-4.17 (m, 2H, C$\mathbf{H_2}$–O); 3.70-3.77 (m, 2H, $CF_2$–$CH_2$–$CH_2$–C$\mathbf{H_2}$–O); 1.86-2.47 (m, aliphatic protons); 1.44 (m, 2H, C$\mathbf{H_2}$-$CH_2$-$CH_2$-O-Ar-N=); 1.28-1.31 (m, 24H, -(C$\mathbf{H_2}$)$_{12}$-$CH_3$); 0.88-0.94 (m, 3H, C$\mathbf{H_3}$). $^{13}$C NMR (50 MHz, $CDCl_3$, TMS) [ppm]: $\delta$ 161.15 (-**C**H=N-), 158.55 (-N=HC-$\mathbf{C_{Ar}}$-O-), 155.51 ($\mathbf{C_{Ar}}$-O-), 143.87 ($\mathbf{C_{Ar}}$-N=CH-), 129.62 ($\mathbf{C_{Ar}}$, orto position to HC=N-), 122.58 ($\mathbf{C_{Ar}}$, orto position to -N=CH-), 115.57 ($\mathbf{C_{Ar}}$, orto position to –O–), 126.09 ($CH_2$-$CF_2$-**C**$F_2$-$CF_2$), 119.76 (**C**$F_2$-$CH_2$), 119.72 (**C**$F_3$), 112.66 (-(**C**$F_2$)$_3$-$CF_2$-$CF_2$-$CF_3$), 108.28 ((**C**$F_2$)$_2$-$CF_3$), 66.40 (**C**$H_2$-O-), 29.50 ((**C**$H_2$)$_{11}$-$(CH_2)_2$-O), 28.56 (**C**$H_2$-$CF_2$-), 25.95 (**C**$H_2$-$CH_2$-O), 22.70 (**C**$H_2$-$CH_3$), 20.33 (-O-$CH_2$-**C**$H_2$-$CH_2$-$CF_2$), 14.11 (**C**$H_3$). Analysis calculated for $C_{40}H_{48}F_{17}NO_2$: C, 53.51%; H, 5.35%; N, 1.56%. Found: C, 53.92%; H, 5.49%; N, 1.62%.

#### *2.3.3 4'-(4 (4,4,5,5,6,6,7,7,8,8,8,9,9,10,10,11,11,11 heptadecafluoroundecyloxy)benzylideneamino) biphenyl-4-carbonitrile* (**3**)

Yield: 90%. Melting point (heating rate 10°C $min^{-1}$): 135°C. FTIR-ATR: $\nu_{max}$ in $cm^{-1}$ 2354, 2326, 2226 (C≡N), 1626 (HC=N), 1603, 1593, 1571, 1510, 1487, 1474, 1420, 1371, 1333, 1307, 1246, 1214, 1195, 1166, 1140, 1115, 1060, 1025, 970, 954, 889, 835, 822, 735, 719, 699. $^1$H NMR (200 MHz, $CDCl_3$, TMS) [ppm]: $\delta$ 8.48 (s, 1H, C**H**=N-); 7.92 (s, 4H, N≡;C-$\mathbf{H_{Ar}}$); 7.65-7.72 (m, 4H, $\mathbf{H_{Ar}}$); 7.34 (s, 2H, $\mathbf{H_{Ar}}$-CH=N-); 7.04 (s, 2H, $\mathbf{H_{Ar}}$-O-); 4.14-4.20 (m, 2H, C$\mathbf{H_2}$–O); 2.44-2.52 (m, 2H, $CH_2$-C$\mathbf{H_2}$– $CH_2$-$CF_2$); 2.13-2.23 (m, 2H, C$\mathbf{H_2}$–$CF_2$). $^{13}$C NMR (50 MHz, $CDCl_3$, TMS) [ppm]: $\delta$ 161.82 (–**C**H=N-), 160.44 ($\mathbf{C_{Ar}}$-O-), 153.14 ($\mathbf{C_{Ar}}$-N=CH-), 145.54 ($\mathbf{C_{Ar}}$-$\mathbf{C_{Ar}}$,), 136.71 ($\mathbf{C_{Ar}}$-$\mathbf{C_{Ar}}$), 133.05 ($\mathbf{C_{Ar}}$, orto position to N≡;C-), 131.16, 129.80, 128.45, ($\mathbf{C_{Ar}}$), 127.82 ($CH_2$-$CF_2$-**C**$F_2$-), 122.09 ($\mathbf{C_{Ar}}$-N=CH=), 120.15 ($CH_2$-**C**$F_2$-$CF_2$-), 119.45 (**C**$F_3$), 115.11 ($\mathbf{C_{Ar}}$, orto position to -O-), 113.58 ($CH_2$-$(CF_2)_2$-(**C**$F_2$)$_3$), 111.05 (**C**$F_2$)$_2$-$CF_3$), 66.89 (**C**$H_2$-O-), 28.78, 28.34, 27.88 ($CH_2$-**C**$H_2$-$CF_2$), 20.97 (-O-$CH_2$-**C**$H_2$-$CH_2$-$CF_2$). Analysis calculated for $C_{31}H_{19}F_{17}N_2O$: C, 49.09%; H, 2.52%; N, 3.69%. Found: C, 48.95%; H, 2.56%; N, 3.68%.

#### *2.3.4 N-(4-(4,4,5,5,6,6,7,7,8,8,8,9,9,10,10,11,11,11 heptadecafluoroundecyloxy)benzylidene) pyren-1-amine* (**4**)

Yield: 89%. Melting point (heating rate 10°C $min^{-1}$): 110°C. FTIR-ATR: $\nu_{max}$ in $cm^{-1}$ 2347, 2326, 1600 (HC=N), 1590, 1513, 1446, 1371, 1330, 1297, 1236, 1191, 1143, 1111, 1060, 1021, 970, 937, 902, 841, 828,

758, 715, 700, 658, 638, 616. $^1$H NMR (200 MHz, $CDCl_3$, TMS) [ppm]: $\delta$ 8.74 (s, 1H, -C**H**=N-); 8.69 (s, 2H, $\mathbf{H_{Ar}}$, pyren structure); 8.00-8.24 (m, 7H, $\mathbf{H_{Ar}}$, pyren structure); 7.89 (s, 2H, $\mathbf{H_{Ar}}$-CH=N-); 7.09 (s, 2H, $\mathbf{H_{Ar}}$-O-); 4.15-4.21 (m, 2H, C$\mathbf{H_2}$–O); 2.17-2.54 (m, 4H, -O-CH$_2$-(C$\mathbf{H_2}$)$_2$-CF$_2$).$^{13}$C NMR (50 MHz, $CDCl_3$, TMS) [ppm]: $\delta$ 162.80 (-**C**H=N-), 160.64 ($\mathbf{C_{Ar}}$-O-), 159.33 ($\mathbf{C_{Ar}}$-N=CH-), 145.31, 145.03, 131.34, 130.87, 130.12, 129.55, 129.39, 128.93, 128.71, 126.64, 125.85, 125.39, 124.89, 124.56, 124, 18, 123.44, 123.06, 122.86 ($\mathbf{C_{Ar}}$, pyren structure), 122.69 (CH$_2$-**C**F$_2$-CF$_2$-), 119.48 (**C**F$_3$), 114.82 ($\mathbf{C_{Ar}}$, orto position to -O-), 113.29 (CH$_2$-(CF$_2$)$_2$-(**C**F$_2$)$_3$), 110.19 (**C**F$_2$)$_2$-CF$_3$), 65.83, 65.94 (**C**H$_2$-O-), 29.51, 29.07, 27.30, 26.84 (CH$_2$-**C**H$_2$-CF$_2$), 19.81 (-O-CH$_2$-**C**H$_2$-CH$_2$-CF$_2$). Analysis calculated for $C_{34}H_{20}F_{17}NO$: C, 52.25%; H, 2.58%; N, 1.79%. Found: C, 52.52%; H, 2.62%; N, 1.81%.

#### *2.3.5 4-((4-(4-(4,4,5,5,6,6,7,7,8,8,9,9,10,10,11,11,11heptadecafluoroundecyloxy)benzylidene-amino)phenyl)diazenyl)-N,N-dimethylbenzenamine* (**5**)

Yield: 86%. Mp. (heating rate 10°C min$^{-1}$): 119°C. FTIR-ATR: $\nu_{max}$ in cm$^{-1}$ 2880, 2348, 2324, 2055, 1600 (HC=N), 1593, 1565, 1513, 1478, 1424, 1362, 1311, 1247, 1211, 1191, 1169, 1140, 1060, 1025, 951, 886, 854, 818, 735, 722, 703. $^1$H NMR (200 MHz, $CDCl_3$, TMS) [ppm]: $\delta$ 8.50 (s, 1H, C**H**=N-); 7.96 (s, 2H, $\mathbf{H_{Ar}}$); 7.91 (s, 2H, $\mathbf{H_{Ar}}$); 7.35 (s, 2H, $\mathbf{H_{Ar}}$); 7.30 (s, 2H, $\mathbf{H_{Ar}}$); 7.10 (s, 2H, $\mathbf{H_{Ar}}$); 6.81 (s, 2H, $\mathbf{H_{Ar}}$); 4.14-4.20 (m, 2H, C$\mathbf{H_2}$–O); 3.14 (s, 6H, (C$\mathbf{H_3}$)$_2$), 2.49-2.52 (m, 4H, CH$_2$-(C$\mathbf{H_2}$)$_2$–CF$_2$). $^{13}$C NMR (50 MHz, $CDCl_3$, TMS) [ppm]: $\delta$ 161.27 (-**C**H=N-), 159.51 ($\mathbf{C_{Ar}}$-O-), 153.06 ($\mathbf{C_{Ar}}$-N=CH-), 152.26, 151.16 ($\mathbf{C_{Ar}}$-N-(CH$_3$)$_2$ and =HC=N-$\mathbf{C_{Ar}}$-N=N-), 143.71 ((CH$_3$)$_2$-N-$\mathbf{C_{Ar}}$-N=N-), 130.69 ($\mathbf{C_{Ar}}$-CH=N-), 129.51 (-O-$\mathbf{C_{Ar}}$, orto position to N=CH), 124.84 (**C**H$_2$-CF$_2$-CF$_2$-), 124.09, 123.26 (-N=N-$\mathbf{C_{Ar}}$-N=CH orto position to N=N and -N-$\mathbf{C_{Ar}}$, orto position to N=N ), 121.54 (CH$_2$-**C**F$_2$-CF$_2$-), 119.04 (**C**F$_3$), 114.53 ($\mathbf{C_{Ar}}$, orto position to -O-), 111.51 (CH$_2$-(CF$_2$)$_2$-(**C**F$_2$)$_3$), 109.05 (**C**F$_2$)$_2$-CF$_3$), 66.41 (**C**H$_2$-O-), 40.32 (**C**H$_3$), 29.71, 28.36 (CH$_2$-**C**H$_2$-CF$_2$), 20.51 (-O-CH$_2$-**C**H$_2$-CH$_2$-CF$_2$). Analysis calculated for $C_{32}H_{25}F_{17}N_4O$: C, 47.77%; H, 3.13%; N, 6.96%. Found: C, 47.82%; H, 3.29%; N, 7.02%.

## 3. Results and discussion

### *3.1 Synthesis and molecular structural characterization*

Azomethines described in this paper were prepared from 4-(4,4,5,5,6,6,7,7,8,8,9,9,10,10,11,11,11-heptadecafluoroundecyloxy)benzaldehyde and five aromatic amines via high-temperature solution condensation in N,N-dimethylacetamide (DMA) at 160°C. Chemical structures of the azomethines (abbreviated hereinafter as **1–5**) are presented in Figure 1, and the details of the synthesis procedures of the azomethines were given in Section 2.

Their expected chemical constitution is clearly confirmed by spectroscopic studies. In particular, in $^{13}$C NMR spectra of the azomethines the signals in the range of 161–163 ppm, present in the spectra of all azomethines, confirmed the existence of the azomethine group carbon atoms (HC=N-). In proton NMR spectra of the investigated compounds, the azomethine proton signal was observed in the range of 8.45–8.74 ppm, as expected. The presence of the azomethine group was also confirmed by FTIR spectroscopy since in each case the band characteristic of the HC=N- stretching deformations was detected. The exact position of this band varies in the spectral range 1600–1626 cm$^{-1}$ (see Section 2). In accordance with the proton and carbon NMR and FTIR spectra collected in Section 2, the spectral data obtained are in agreement with the spectral data predicted from the chemical formulae of the synthesized compounds.

Also, the mass dispersion of the **1–5** molecules was examined using a SEC method (polystyrene standards were used). A single narrow SEC band found for the

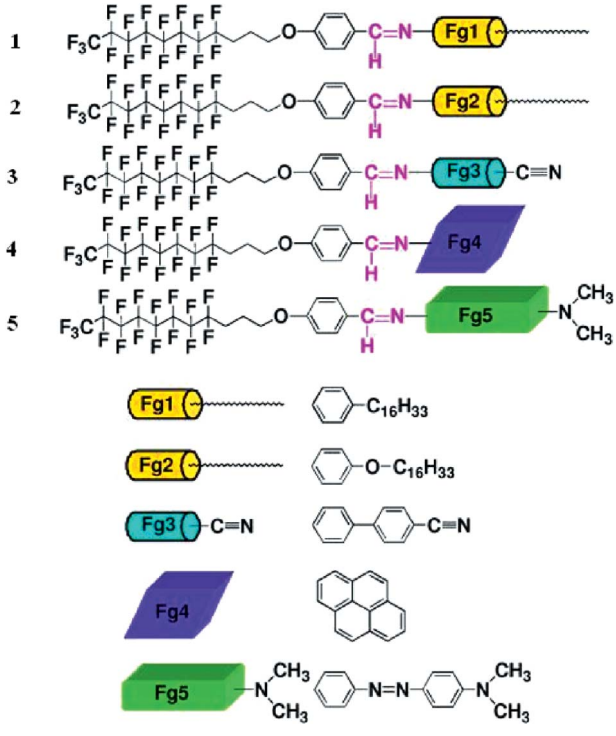


Figure 1. Chemical structure of the synthesized azomethines.

each azomethine tested (not showed here) clearly indicated a mono-dispersive distribution of the azomethines molecular masses and thereby additionally provided evidence of the high purity of the compounds synthesized.

The UV-vis (absorbance) spectra of the compounds in THF solution display two absorption maxima in the region 280–290 nm (4.43–4.28 eV) and 324–428 nm (3.83–2.90 eV). The former band can be assigned to a $\pi$–$\pi^*$ transition whereas the second band is characteristic to the azomethine group in the compounds **1–5** and its position and intensity are highly dependent on the chemical constitution of the compound (Figure 2(a)). In particular, for the azomethines with aliphatic segments (**1** and **2**) the band attributed to azomethine chromophore is hypsochromically shifted as compared with the analogous band in compounds with no aliphatic sub-units. The introduction of an azo spacer (-N=N-) between the phenylene rings of, for example, the transformation of **3** into **5** results in a bathochromic shift of the absorption band of the azomethine group from 320 to 428 nm. Also the incorporation of the pyren group to the azomethine structure causes red shifts of the second absorption band to 384 nm, that is, in between those of the azomethines **3** and **4**. For all of the compounds the fluorescence (emission) spectra in THF solution at room temperature (~25°C) were recorded for the excitation wavelength 325 nm. The compounds exhibit one emission band under 325 nm excitation wavelengths. In addition, for the azomethine **5** under 360 nm excitation wavelengths the second emission band at about 516 nm was observed and exhibited very low intensity. The maximum of the emission band of the investigated compounds increased in the following order: 359 nm (**5**) < 360 nm (**1**) < 373 nm (**2**) < 414 nm (**3**) < 451 nm (**5**). It is apparent that a bathochromic effect (red shift) occurs with the introduction of an oxygen atom (compare compounds **1** and **2**), biphenyl-4-carbonitrile or pyrene moieties (compare compounds **1** and **3** or **4**). Fluorescence spectra of some azomethines are presented in Figure 2(b) as an example.

Current–voltage curves of the ITO/compound/$Alq_3$/Al are shown in Figure 3. It can be seen that current increases with applied voltage increase. The turn-on voltage of the devices was observed at about 6 V in room temperature for the compounds **1–3** and at about 8 V for the compound **4**. The value of conductivity of the investigated compounds **1–4** was about $10^{-8}$–$10^{-7}$ S m$^{-1}$ for voltage 6–8 V (see Figure 3), which categorizes probe materials between semiconductors and dielectrics (*39, 43, 44*). Different types of conjugated polymers such as polyacetylene, poly(p-phenylene), poly(p-phenylenevinylene) (PPV),

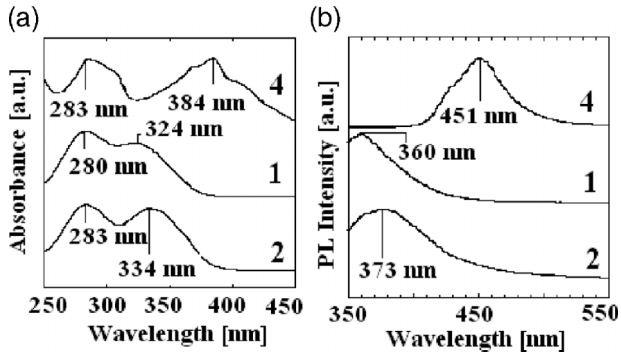


Figure 2. UV-vis absorption and fluorescence emission spectra of the azomethines **1**, **2** and **4** in THF solution.

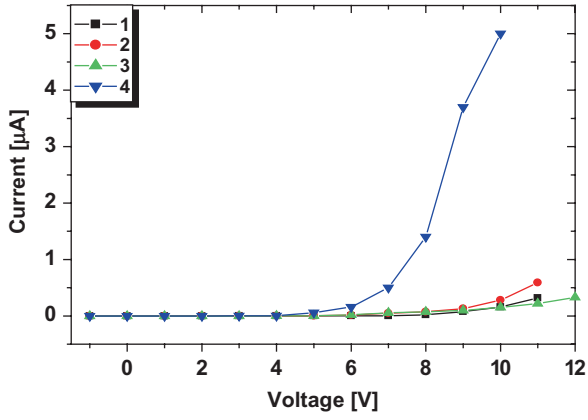


Figure 3. Current–voltage curves of the ITO/azomethine/$Alq_3$/Al devices.

polyaniline (PANI), polypyrrole and polythiophene have been developed and investigated intensively as organic semiconductors (*43, 45–50*). For example, the conductivity of polyacetylene is $10^{-6}$ S m$^{-1}$ for *trans* form and $10^{-11}$ S m$^{-1}$ for *cis* form (*46*). After redox-type doping the conductivity of polyacetylene increased as high as $10^3$ S m$^{-1}$ (see (*46*)). On the other hand, the conductivity of poly(3-alkylthiophene) before doping was $10^{-11}$ S m$^{-1}$, while after doping it was 10 S m$^{-1}$ (see (*47, 48*)). PPV has conductivity higher than 1 S m$^{-1}$ (see (*49*)). PANI after doping could have conductivity as high as 10 S m$^{-1}$ (see (*43, 50*)). Concerning the electrical properties of the polyazomethines it should be stressed that the conductivities of undoped polymers are low, but doping causes an increase of the conductivity (*51*). The conductivity of the undoped polyazomethines was in the range $10^{-16}$–$10^{-11}$ S m$^{-1}$ (see (*51*)). After doping the conductivity of the polyazomethines increased to as high as $10^{-9}$ S m$^{-1}$ (see (*51*)).

In addition, it should be mentioned that the first conjugated polymer used for the fabrication of an organic light emitting diode (OLED) was PPV (*45, 49*). With the device configuration ITO/PPV/Al, substantial charge injection was observed just below 14 V. The turn-on voltage of the devices ITO/PAZ-TPA/$Alq_3$/Al was observed at about 6 V. We found no significant differences between current–voltage characteristic of our azomethines and polyazomethines with triphenylamine core (PAZ-TPA) in the main chain (*52*).

### 3.2 *Mesomorphic behaviour*

All compounds were studied using DSC and POM methods to determine their mesomorphic properties. First, one may accept that upon the DSC/POM analysis the compounds exhibited a complex mesomorphic transition behaviour, that is, the crystal-to-mesophase (Cr/M), mesophase-to-mesophase (M/M) and mesophase-to-isotropic (M/I) transitions. The POM and DSC observations revealed that all of the compounds were enantiotropic LCs. Azomethines **1**, **3** and **5** exhibited two phases (smectic C (SmC) and smectic A (SmA) or smectic X (SmX) and SmA). In contrast, the azomethine **2** exhibited three enantiotropic smectic phases, which implies a significant effect of the oxygen atom on the mesomorphic properties. Different behaviour was also observed for the compound **4**. In this case only one smectic phase (SmA) was found, characterized by the formation of the typical focal conic fan-like texture (Figure 4).

The details of transition temperatures of the compounds as determined by POM are summarized in Table 1 together with their phase variants. The transition temperatures and enthalpies of the azomethines **1–5** determined by DSC are presented in Table 2. DSC thermograms of the azomethines **1** and **2** obtained on the second heating and the second cooling, under $N_2$ atmosphere are shown in Figure 5.

Tables 1 and 2 reveal that the compounds **3–5** exhibited a clearing point temperature higher than 250°C and broad thermal range of the mesophase. For example, the thermal range of the SmA phase of compound **3** exceeds 190°C and that of the mesophase of the azomethine **4** exceeds 146°C (see Table 1). On the other hand, the compounds **1** and **2** have a clearing point temperature at about 140°C and narrow thermal range of the mesophase (Figure 5). For the investigated azomethines different mesomorphic properties were observed (see Tables 1 and 2 and Figures 4 and 6). This behaviour indicates the role of the rigid mesogenic core structure in creating their mesomorphic properties.

It is also worth noting that in accordance with the results of DSC measurements the melting

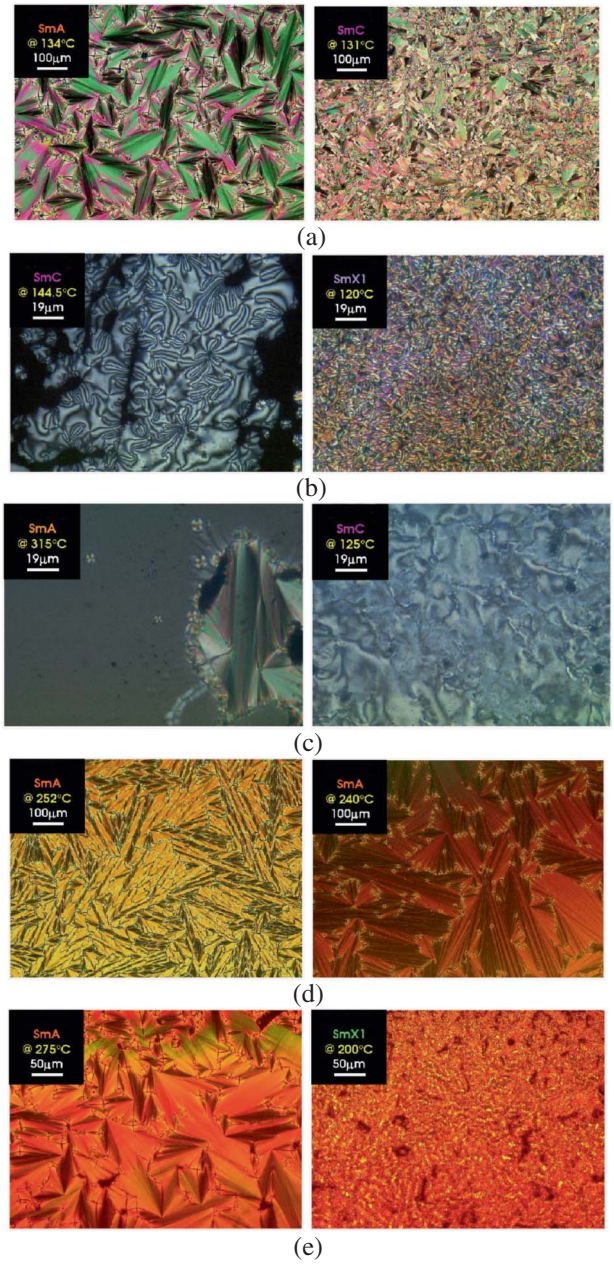


Figure 4. Polarized light micrograph of the all azomethines (cross-polarization position).

Table 1. Phase transition temperature (°C) of the compounds detected by POM.

| Code | Phase transitions, cooling, POM |
|---|---|
| **1** | Cr 107, SmC 129, SmA 131, I |
| **2** | Cr 106, SmX2 110, SmX1 113, SmC 140, I |
| **3** | Cr 110, SmC 130, SmA 320, I |
| **4** | Cr 107, SmA 253, I |
| **5** | Cr 115, SmX1 240, SmA 290, I |

Cr, SmA, SmC, SmX and I indicate crystal, smectic A, smectic C, smectic X and isotropic phases, respectively.

Table 2. Transition temperatures and enthalpies of the azomethines detected by DSC.

| Code | Phase transitions (° C) (with corresponding enthalpy changes in parentheses in J $g^{-1}$) | |
|---|---|---|
| | Heating | Cooling |
| **1** | 108.3 (15.08), 128.9 (2.68), 131.9 (13.00) | 106.9 (14.55), 128.7 (2.62), 131.5 (12.70) |
| **2** | 109.0 (138.84), 111.3 (0.22), 113.9 (10.17), 142.1 (15.17) | 105.9 (13.01), 110.3 (0.1), 113.2 (10.59), 141.2 (15.2) |
| **3** | 135.0 (33.55), 309.7 (11.50) | 106.9 (23.71), 309.9 (7.00) |
| **4** | 106.1 (22.52), 250.3 (4.78) | 46.9 (7.69), 56.1 (1.60), 250.2 (4.69) |
| **5** | 118.7 (11.17), 202.2 (4.77), 297.4 (8.59) | 93.7 (5.58), 200.5 (1.59), 296.9 (8.51) |



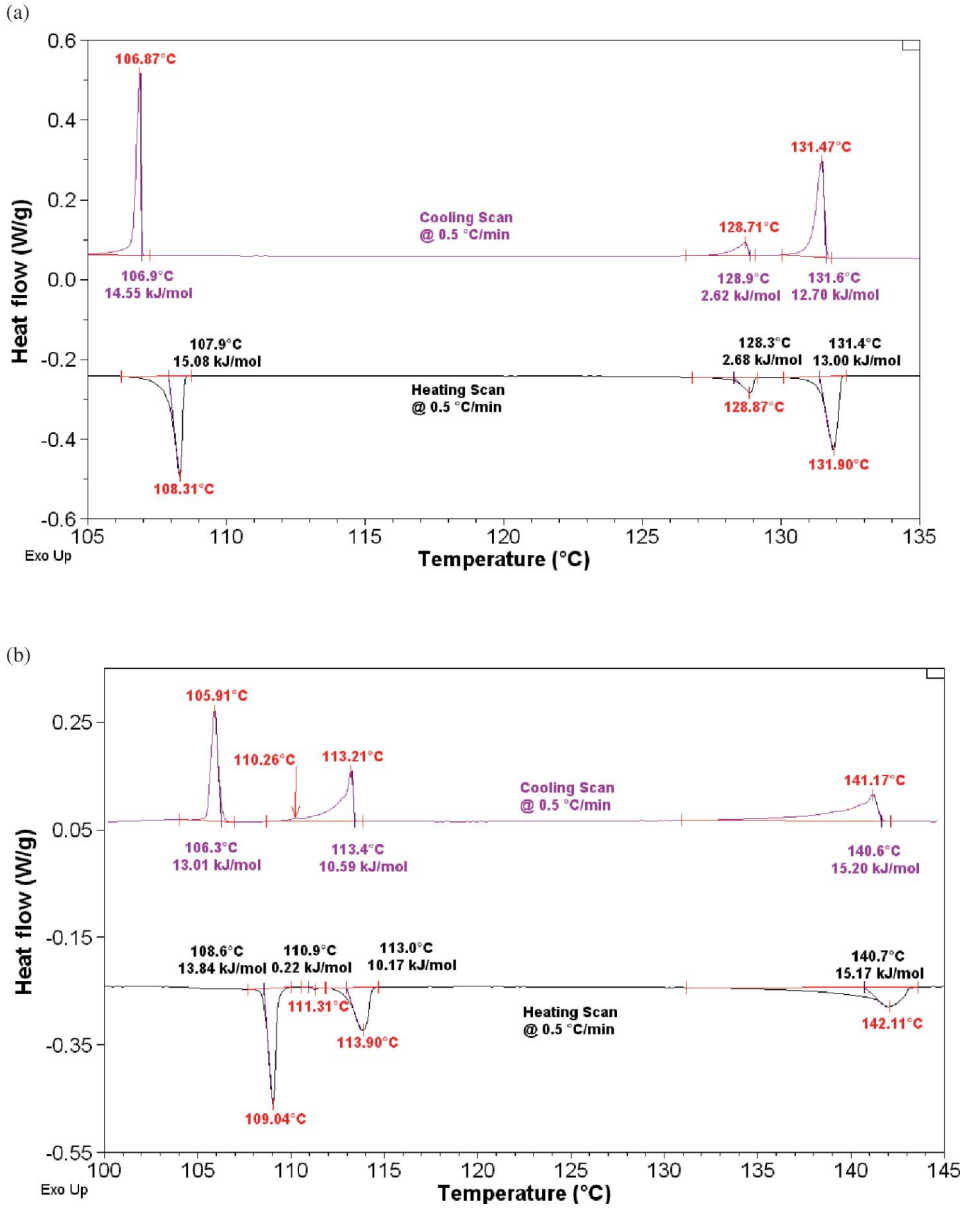


Figure 5. DSC traces of the (a) azomethine **1** and (b) azomethine **2** obtained on the second heating and the first cooling, with a heating and cooling rate of 0.5°C $min^{-1}$ under $N_2$ atmosphere.

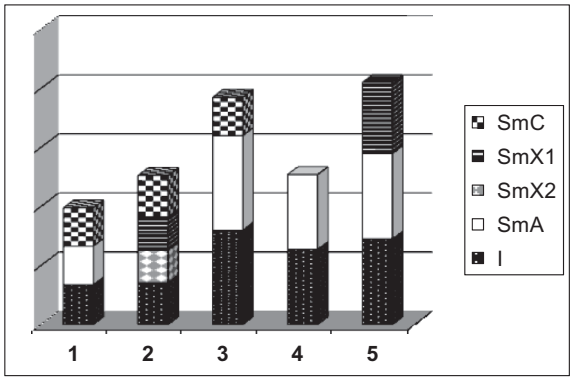


Figure 6. Graphs showing the phase behaviour of the compounds.

temperatures increased distinctly in the following order: 106°C (**4**) < 108°C (**1**) < 109°C (**2**) < 118°C (**5**) < 135°C (**3**). Different behaviour was observed for the clearing temperature of the azomethines and upon the initiation of the heating cycle they were ordered as 132°C (**1**) < 142°C (**2**) < 250°C (**4**) < 297°C (**5**) < 310°C (**3**).

It should also be noted that the phase transition temperature values noted in the DSC thermograms were almost equivalent to those of the transition temperatures estimated from POM investigations.

### *3.3 FTIR-ATR(T) studies*

FTIR spectroscopy provides detailed information about the orientational distributions of specific functional groups in oriented liquid crystal samples, and thus in principle represents a powerful probe of microscopic ordering in liquid crystals (*53–56*). The thermotropic phase behaviour of the selected azomethines was additionally investigated at different temperatures by using temperature-dependent FTIR spectra. Changes in absorbance related to reorientation of the molecules at the phase transitions were observed. Figure 7 shows the temperature dependence of the FTIR spectra of the azomethines **1** and **2**, as example, in the cooling process from the isotropic state. The stretching vibration bands characteristic of the alkyl spacer appeared in room temperature at 2918 and 2850 $cm^{-1}$ for the compounds **1** and **2** (see Fig. 7).

The vibration bands of the alkyl spacer can be assigned to the antisymmetric and symmetric $CH_2$ vibration. It is known that the frequencies of the bands due to the $CH_2$ antisymmetric and symmetric modes of the alkyl chain usually appear at 2915 and 2850 $cm^{-1}$, corresponding to highly ordered hydrocarbon chains with an all-*trans* conformation (*35, 36*). All of the $CH_2$ antisymmetric and symmetric vibrations in the case of the azomethines **1** and **2** appeared at about

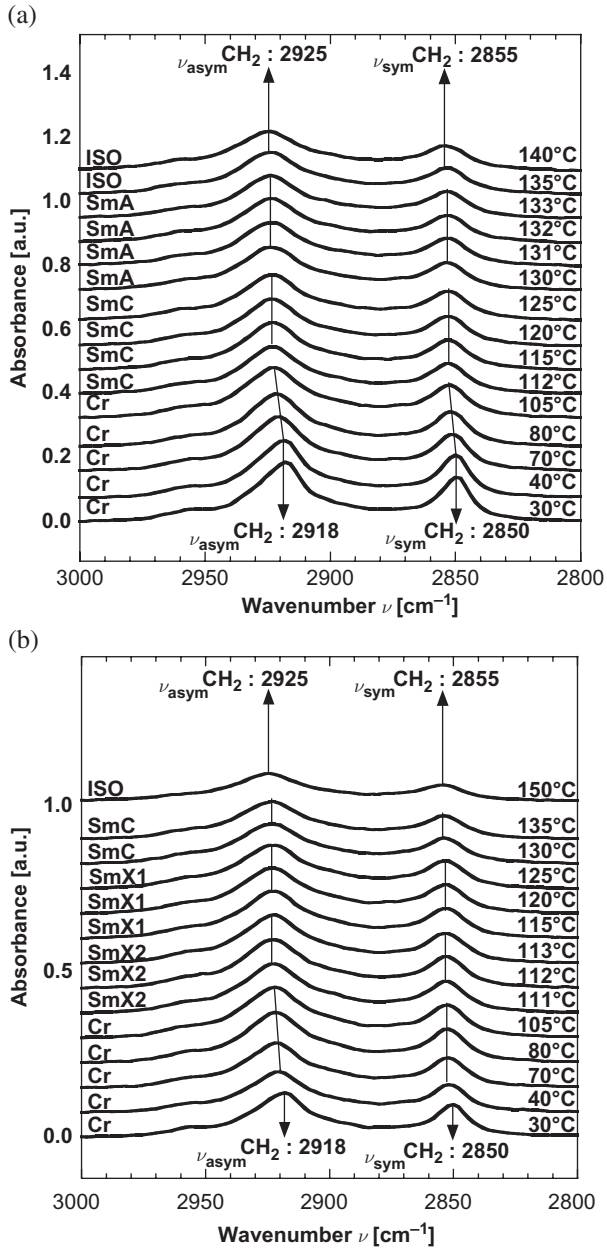


Figure 7. Temperature dependence of FTIR spectra between 2800 and 3000 $cm^{-1}$ of (a) azomethine **1** and (b) azomethine **2**.

these frequencies, indicating the existence of *trans* isomers in the hydrocarbon chains. The temperature dependences of the peak frequency of these bands are shown in Figure 8.

The $CH_2$ stretching vibration shifts to the lower frequency on decreasing temperature from the isotropic state of the compounds **1** and **2**. When the temperature reaches the crystalline phase transition point at 105°C, the frequency decreases by about 7 $cm^{-1}$ for antisymmetric $CH_2$ stretching vibration and 5 $cm^{-1}$ for

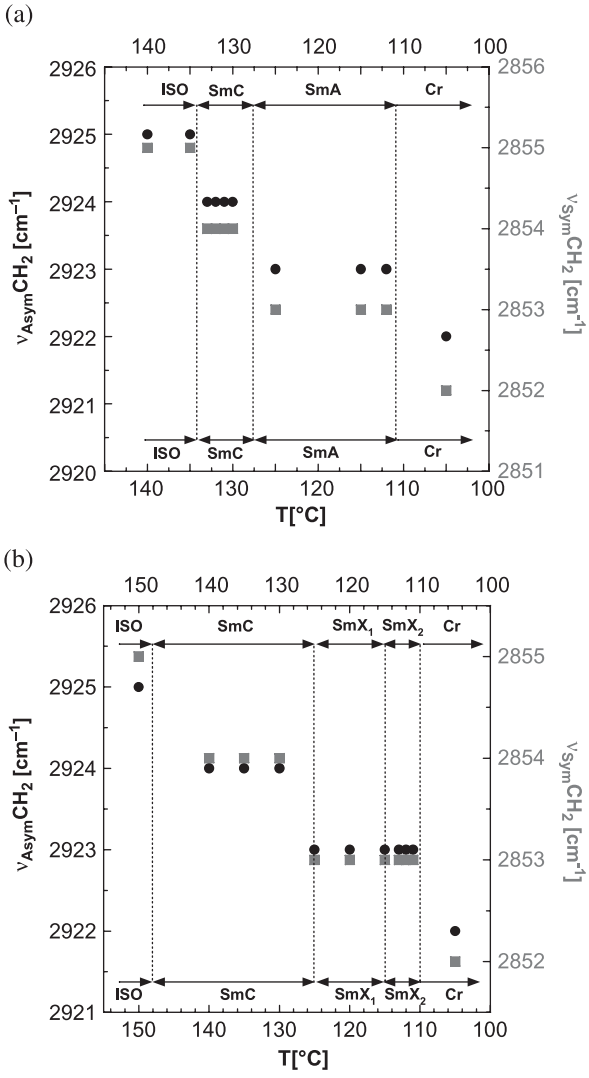


Figure 8. Temperature dependence of the antisymmetric and symmetric $CH_2$ stretching vibrational frequencies in (a) azomethine **1** and (b) azomethine **2**.

symmetric $CH_2$ stretching vibration. In the temperature region above this transition point, the vibration frequency decreases slowly. The antisymmetric and symmetric $CH_2$ stretching vibrations of the azomethine **1** shift at 133°C from 2925 to 2924 cm$^{-1}$ and from 2855 to 2854 cm$^{-1}$, respectively, which corresponds to the Iso–SmA phase transition temperature. When decreasing temperature, the antisymmetric and symmetric $CH_2$ stretching vibrations of the compound **1** changes the position at 125°C from 2924 to 2923 cm$^{-1}$ and from 2854 to 2852 cm$^{-1}$, respectively (SmA–SmC) and to 2918 and 2850 cm$^{-1}$, at 105°C (SmC–Cr). The antisymmetric and symmetric $CH_2$ stretching vibrations of the azomethine **2** show temperature dependences similar to that of the azomethine **1** (Figure 7).

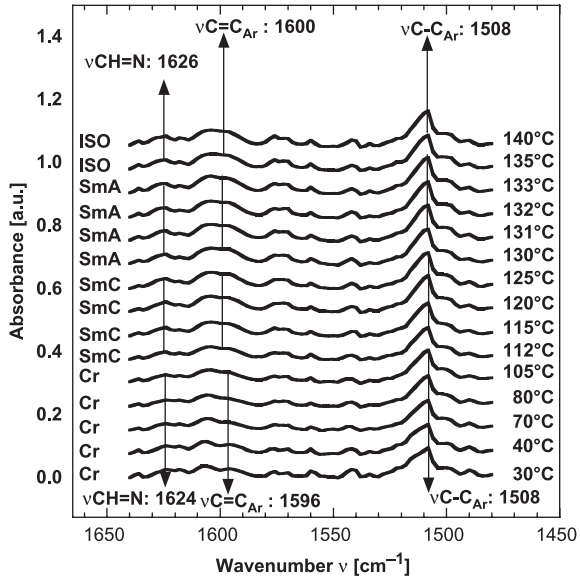


Figure 9. Temperature dependence of FTIR spectra between 1450 and 1650 cm$^{-1}$ of the compound **1**.

The bands characteristic of azomethine are detected in the wavenumber region between 1450 and 1650 cm$^{-1}$. The HC=N-, C=$C_{ar}$ and C–$C_{ar}$ stretching vibrations are located near 1624, 1596 and 1508 cm$^{-1}$, respectively. The temperature dependences of the FTIR spectra of the azomethine **1** in the cooling process from the isotropic state are present in Figure 9.

The HC=N and C=$C_{ar}$ stretching vibrations decreases slowly to the lover frequency on decreasing the temperature (Figure 9).

The results show that the aliphatic chain is more sensitive to the crystal–liquid crystal transitions than the imine bond.

### *3.4 UV-vis(T) studies*

Figure 10 shows the temperature dependence of the UV-vis spectra of the compound **5**, as example, in a temperature range from the room temperature to clearing point in the heating process.

Using UV-vis spectroscopy to monitor the changes in spectroscopic properties of the azomethine **5** during heating, we observed three changes in the position of the isosbestic point, indicating that the differential transitions proceeds not randomly but stepwise. An isosbestic point appears when a compound is quantitatively transformed from crystal to one mesophase and later into another during heating, so the three different isosbestic points observed suggest that three different transitions are formed successively.

UV-vis spectra of the azomethine **5** during heating changed in three ranges: range I, 25–135°C; range II, 150–241°C; and range III, 250–292°C (Figure 10).

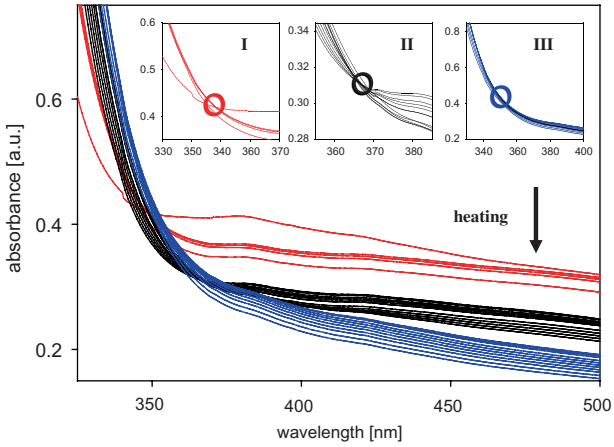


Figure 10. Temperature dependence of UV-vis spectra of the azomethine **5** in the following temperatures: range I, 25, 115, 120, 125 and 135°C; range II: 150, 170, 190, 200, 210, 220, 235, 236, 238, 239, 240 and 241°C; range III: 250, 260, 270, 285, 286, 287, 288, 289, 290, 291 and 292°C. Insets: (a) The isosbestic point at 350 nm (115–135°C); (b) the isosbestic point at 368 nm (150–241°C); and (c) the isosbestic point at 350 nm (250–292°C).

Also in UV-vis spectra of the azomethine **5** the hipochromic effect along with increase the temperature was observed. The absorption band around 378 nm at 25°C is about 7 nm bathochromically shift along with an increase in the temperature to 190°C and is observed at this position to 220°C (385 nm). At 235°C the absorption band at 385 nm is observed at this position to 285°C and at 286°C is red shift to 387 nm which corresponds to the transition SmX1–SmA. The absorption properties of the azomethine **5** on the glass during heating the sample from room temperature to the clearing point in the selected temperatures are presented in Figure 11.

The spectra of the azomethine **5** gradually changed, with an isosbestic point at 350 and 368 nm due to an increase in the temperature from 25 to 292°C (Figure 10, inset). The isosbestic point at 350 nm appears in the temperature range 115–135°C and is about a 28 nm blue shift in comparison with the second isosbestic point observed in the temperature range 150–241°C (Figure 11, first and second inset). The third isosbestic point observed at 350 nm (250–292°C) is a 16 nm blue shift in comparison with the second isosbestic point.

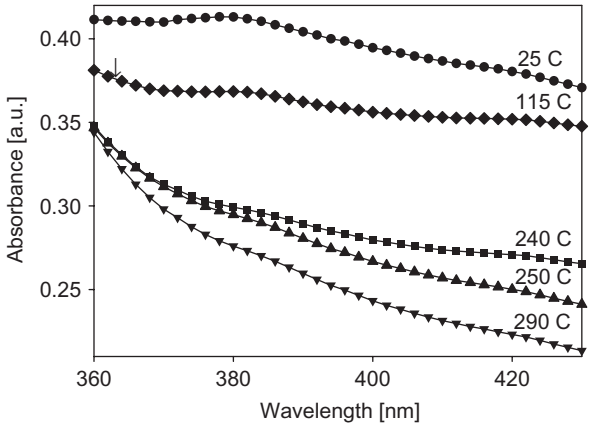


Figure 11. UV-vis spectra of the azomethine **5** in the selected temperatures.

## 4. Conclusion

In summary, we prepared a series of liquid crystalline azomethines by the condensation of 4-(4,4,5,5,6,6,7,7,8,8,9,9,10,10,11,11,11-heptadecafluoroundecyloxy) benzaldehyde with aliphatic and aromatic amines.

The following conclusions can be drawn from the present work.

(1) Five new unsymmetrical azomethines containing a mesogenic unit have been synthesized and characterized. The molecular structures were identified by FTIR, NMR spectroscopy and elemental analysis, and the results were in accordance with the expected molecular formulae.
(2) All of the compounds were crystalline. The values of melting points were in the range 110–135°C.
(3) All azomethines showed the smectic mesomorphism. The mesophases of the azomethines **1** and **3** have been designated to be SmC and SmA phases. Azomethine **4** showed a SmA phase, while compound **5** has an additional SmX1 phase. The rich polymorphism of the azomethine **2** was found.
(4) The photoluminescence properties under 325 nm excitation wavelength exhibit all azomethines. The maximum of the emission band of the investigated compounds increase in the following order: 359 nm (**5**) < 360 nm (**1**) < 373 nm (**2**) < 414 nm (**3**) < 451 nm (**5**).
(5) Preliminary investigations of the current–voltage characteristics for a device such as ITO/azomethine/$Alq_3$/Al confirmed their semiconductivity properties of the organic thin film.

## Acknowledgement

The first author expresses her gratitude to the Chemistry Department of CNRS for the funding of her one-year postdoctoral fellowship within UMR5819-SPrAM Lab (Grenoble, France).

## References

(1) Broer, D.J.; van Haaren, J.A.M.M.; Bastiaansen, C.W.M. *e-Polymers*, **2001**, *023*.

(2) Collyer, A.A. (ed.). *Liquid Crystal Polymers: From Structures to Applications*; Elsevier/The Society of Materials Sciences, Japan, 1992.
(3) Hird, M. *Chem. Soc. Rev.* **2007**, *36*, 2070–2095.
(4) Kirsch, P.; Bremer, M.; Heckmeier, M.; Tarumi, K. *Angew. Chem., Int. Ed.* **1999**, *38*, 1989–1992.
(5) Smith, J.A.; DiStasio, R.A.; Hannah, N.A.; Winter, R.W.; Weakley, T.J.R.; Gard, G.L.; Rananavare, S.B. *J. Phys. Chem. B.* **2004**, *108*, 19940–19948.
(6) Nadasi, H.; Weissflog, W.; Eremin, A.; Pelzl, G.; Diele, S.; Das, B.; Grande, S. *J. Mater. Chem.* **2002**, *12*, 1316–1324.
(7) Nastishin, Y.A.; Achard, M.F.; Nguyen, H.T.; Kleman, M. *Eur. Phys. J. E* **2003**, *12*, 581–591.
(8) Takezoe, H.; Takanishi, Y. *Jpn. J. Appl. Phys.* **2006**, *45*, 597–625.
(9) Reddy, R.A.; Tschierske, C. *J. Mater. Chem.* **2006**, *16*, 907–961.
(10) Bilgin-Eran, B.; Yorur, C.; Tschierske, C.; Prehm, M.; Baumeister, U. *J. Mater. Chem.* **2007**, *17*, 2319–2328.
(11) Neubert, M.E.; Keast, S.S.; Law, C.C.; Lohman, M.C.; Bhatt, J.C. *Liq. Cryst.* **2005**, *32*, 781–795.
(12) Sakaigawa, A.; Nohira, H. *Ferroelectrics* **1993**, *148*, 71–78.
(13) Drzewinski, W.; Czuprymski, K.; Dabrowski, R.; Neubert, M. *Mol. Cryst. Liq. Cryst.* **1999**, *328*, 401–410.
(14) Stipetic, A.I.; Goodby, J.W.; Hird, M.; Raoul, Y.M.; Gleeson, H.F. *Liq. Cryst.* **2006**, *33*, 819–828.
(15) Cowling, S.J.; Hall, A.W.; Goodby, J.W.; Wang, Y.; Gleeson, H.F. *J. Mater. Chem.* **2006**, *16*, 2181–2191.
(16) Wu, S.; Lin, C. *Liq. Cryst.* **2005**, *32*, 1053–1059.
(17) Liu, H.; Nohira, H. *Liq. Cryst.* **1996**, *20*, 581–586.
(18) Takenaka, S. *J. Chem. Soc., Chem. Commun.* **1992**, 1748–1749.
(19) Bao, X.; Dix, L.R. *Mol. Cryst. Liq. Cryst.* **1996**, *281*, 291–294.
(20) Mori, A.; Uno, K.; Takeshita, H.; Takematsu, S. *Liq. Cryst.* **2005**, *32*, 107–113.
(21) Tournilhac, F.; Bilnov, L.M.; Simon, J.; Yablonsky, S.V. *Nature* **1992**, *359*, 621–623.
(22) Hird, M.; Goodby, J.W.; Gough, N.; Toyne, K.J. *J. Mater. Chem.* **2001**, *11*, 2732–2742.
(23) Glebowska, A.; Przybylski, P.; Winek, M.; Krzyczkowska, P.; Krowczynski, A.; Szydlowska, J.; Pociecha, D.; Gorecka, E. *J. Mater. Chem.* **2009**, *19*, 1359–1398.
(24) Dahn, U.; Erdelen, C.; Ringsdorf, H.; Festag, R.; Wendorff, J.H.; Heiney, P.A.; Maliszewskyj, N.C. *Liq. Cryst.* **1995**, *19*, 759–764.
(25) Terasawa, N.; Monobe, H.; Kiyohara, K.; Shimizu, Y. *Chem. Commun.* **2003**, 1678–1679.
(26) Alameddine, B.; Aebischer, O.F.; Amrein, W.; Donnio, B.; Deschenaux, R.; Guillon, D.; Savary, C.; Scanu, D.; Scheidegger, O.; Jenny, T.A. *Chem. Mater.* **2005**, *17*, 4798–4807.
(27) Kouwer, P.H.J.; Picken, S.J.; Mehl, G.H. *J. Mater. Chem.* **2007**, *17*, 4196–4203.
(28) Percec, V.; Imam, M.R.; Bera, T.K.; Balagurusamy, V.S.K.; Peterca, M.; Heiney, P.A. *Angew. Chem. Int. Ed.* **2005**, *44*, 4739–4745.
(29) Yoon, D.K.; Lee, S.R.; Kim, Y.H.; Choi, S.-M.; Jung, H.-T. *Adv. Mater.* **2006**, *18*, 509–513.
(30) Percec, V.; Glodde, M.; Johansson, G.; Balagurusamy, S.K.; Heiney, P.A. *Angew. Chem., Int. Ed.* **2003**, *42*, 4338–4342.
(31) Percec, V.; Glodde, M.; Peterca, M.; Rapp, A.; Schnell, I.; Spiess, H.W.; Bera, T.K.; Miura, Y.; Balagurusamy, S.K.; Aqad, E.; Heiney, P.A. *Chem. Eur. J.* **2006**, *12*, 6298–6314.
(32) Yamaguchi, A.; Maeda, Y.; Yokoyama, H.; Yoshizawa, A. *Chem. Mater.* **2006**, *18*, 5704–5710.
(33) Rabolt, J.F.; Russell, T.P.; Twieg, R.J. *Macromolecules* **1984**, *17*, 2786–2794.
(34) Ropers, M.H.; Stebe, M.J. *Phys. Chem. Chem. Phys.* **2001**, *3*, 4029–4036.
(35) Regev, O.; Leaver, M.S.; Zhou, R.; Puntambekar, S. *Langmuir* **2001**, *17*, 5141–5149.
(36) Rankin, S.E.; Tan, B.; Lehmler, H.; Hindman, K.P.; Knutson, B.L. *Microporous Mesoporous Mater.* **2004**, *73*, 197–202.
(37) Acimis, M.; Karaman, E.B. *J. Colloid Interface Sci.* **2006**, *300*, 1–6.
(38) Kato, T.; Mizoshita, N.; Kishimoto, K. *Angew. Chem. Int. Ed.* **2006**, *45*, 38–68.
(39) Kato, T.; Yasuda, T.; Kamikawa, Y.; Yoshio, M. *Chem. Commun.* **2009**, 729–739.
(40) Kirsch, P.; Binder, W.; Hahn, A.; Jahrling, K.; Lenges, M.; Lietzau, L.; Maillard, D.; Meyer, V.; Poetsch, E.; Ruhl, A.; Unger, G.; Frohlich, R. *Eur. J. Org. Chem.* **2008**, 3479–3487.
(41) Tschierske, C. *Chem. Soc. Rev.* **2007**, *36*, 1930–1970.
(42) Imrie, C.T.; Henderson, P.A. *Chem. Soc. Rev.* **2007**, *36*, 2096–2124.
(43) Pron, A.; Rannou, P. *Prog. Polym. Sci.* **2002**, *27*, 135–190.
(44) Frechet, J.M.J. *Prog. Polym. Sci.* **2005**, *30*, 844–857.
(45) Mitschke, U.; Bauerle, P. *J. Mater. Chem.* **2000**, *10*, 1471–1507.
(46) Shirakawa, H.; Louis, E.J.; Mac-Diarmid, A.G.; Chiang, C.K.; Hegger, A. *J. Chem. Soc. Chem. Commun.* **1977**, *16*, 578–579.
(47) Jen, K.Y.; Miller, G.C.; Elsenbaumer, R.L. *J. Chem. Soc., Chem. Commun*. **1986**, *17*, 1346–1347.
(48) Elsenbaumer, R.L.; Jen, K.Y.; Oboodi, R. *Synth. Met.* **1986**, *15*, 169–174.
(49) Elsworth, Y.; Howe, R.; Isaak, G.R.; McLeod, C.P.; New, R. *Nature* **1990**, *347*, 536–539.
(50) Cao, Y.; Smith, P.; Heeger, A.J. *Synth. Metals* **1992**, *48*, 91–97.
(51) Iwan, A.; Sek, D. *Prog. Polym. Sci.* **2008**, *33*, 289–345.
(52) Sek, D.; Iwan, A.; Jarzabek, B.; Kaczmarczyk, B.; Kasperczyk, J.; Mazurak, Z.; Domanski, M.; Karon, K.; Lapkowski, M. *Macromolecules* **2008**, *41*, 6653–6663.
(53) David, C.; Baeyens-Volant, D. *Liq. Cryst.* **1989**, *6*, 247–261.
(54) Matsui, E.; Nito, K.; Yasuda, A. *Liq. Cryst.* **1994**, *17*, 311–322.
(55) Tian, Y.; Xu, X.; Zhao, Y.; Tang, X.; Li, T.; Sun, J.; Li, C.; Pan, A. *Thin Solid Films* **1996**, *284–285*, 603–605.
(56) Moriya, K.; Mizusaki, H.; Kato, M.; Suzuki, T.; Yano, S.; Kajiwara, M.; Tashiro, K. *Chem. Mater.* **1997**, *9*, 255–263.